NJC

ROYAL SOCIETY OF CHEMISTRY

PAPER

View Article Online
View Journal | View Issue

Cite this: *New J. Chem.*, 2024, **48**, 14873

Exploring the interaction of decavanadate with methylene blue, toluidine blue and rhodamine B†

Juliana M. Missina, ‡[a] Heloísa de S. Camilo, ‡[a] Rúbia C. R. Bottini, [a] Isabela P. S. Silva, [a] Lucas G. Fachini, [a] Patrizia Rossi, [b] Paola Paoli, [b] Eduardo L. de Sá [a] and Giovana G. Nunes *[a]

The interaction of decavanadate with the cationic organic dyes methylene blue (MB), toluidine blue (TB) and rhodamine B (RB) was explored. For that purpose, a novel decavanadate salt $(2,3\text{-ampH})_6[V_{10}O_{28}]\cdot 4H_2O$ (**2,3-ampV$_{10}$**), where 2,3-ampH$^+$ = 2-amino-3-methylpyridinium, and two salts with the organic dyes $(MB)_4[H_2V_{10}O_{28}]\cdot 10.8H_2O$ (**MBV$_{10}$**) and $(TB)_4(H_2V_{10}O_{28})\cdot 10H_2O$ (**TBV$_{10}$**) were synthesized. The compounds were characterized by elemental analysis, powder X-ray diffraction, energy dispersive X-ray spectroscopy, scanning electron microscopy and infrared spectroscopy. The salts **2,3-ampV$_{10}$** and **MBV$_{10}$** were also characterized by single-crystal X-ray diffraction, while **TBV$_{10}$** was isolated as an amorphous solid. The supramolecular features of **MBV$_{10}$** showed columns of MB cations connected to V_{10} through H-bond interactions that resulted in channels filled with water molecules. The absorption spectrum of **MBV$_{10}$** was studied by density functional theory (DFT) calculations at the X3LYP/def2-TZVP level using the crystallographic data. The efficacy of **2,3-ampV$_{10}$** to bleach MB solutions at pH 6.2–6.5 was outstanding, achieving nearly 90% discoloration in only 5 min, presenting moderate efficacy towards TB and quite negligible towards RB. Moreover, a metachromatic effect was observed in the TB solution at pH 3. The IR spectra of the isolated solids and the mass spectra of the supernatants suggest both adsorption and cation exchange as the main responsible processes for the bleaching of MB and TB solutions. The present work has tackled many fronts related to the chemistry of POVs, mainly synthetic, structural, and environmental approaches.

Received 28th May 2024,
Accepted 29th July 2024

DOI: 10.1039/d4nj02454k

rsc.li/njc

Introduction

The use of organic dyes to impart color to textiles, leather, food products, or other materials enormously impacts water bodies, as approximately 10–15% of the waste from industries is discharged into water systems without treatment.[1] Polyoxidometalates (POMs), mainly those based on molybdenum and tungsten, have been broadly explored for dye removal by adsorption and photocatalytic degradation due to the high efficiency achieved using simple and low-cost procedures.[2] Among others, methylene blue (MB), a dye belonging to the thiazine family, and rhodamine B (RB), a dye that belongs to the xanthene family (Chart 1), have worked as good models to test the color-removal ability of various POMs in aqueous media.[3]

A mechanism of MB adsorption on the surface of the commercial polyoxidomolybdate $[Mo_7O_{24}]^{6-}$ was proposed by Sabarinathan *et al.*[4] In acidic medium, there is a higher degree of protonation of the polyoxidoanion, favoring olation reactions that generate an additional negative charge on the POM. This additional negative charge promoted the adsorption of MB cations on the POM surface, which is regenerated for further adsorption reactions in the presence of tetrabutylammonium cations.[4]

Polyoxidovanadates (POVs) are high-nuclearity negatively-charged vanadium oxides that have been assessed for a number of purposes, such as in biomedicine,[5] magnetism,[6] energy

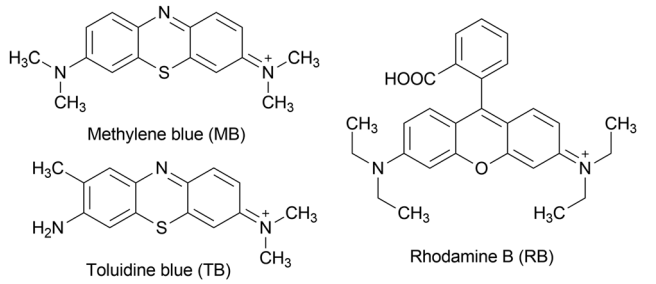

Chart 1 Structural formulas of the dyes.

[a] *Departamento de Química, Universidade Federal do Paraná, Curitiba, PR, Brazil. E-mail: nunesgg@ufpr.br*
[b] *Dipartimento di Ingegneria Industriale, Università degli Studi di Firenze, Firenze, Italy*

† Electronic supplementary information (ESI) available. CCDC 2357605 and 2357606. For ESI and crystallographic data in CIF or other electronic format see DOI: https://doi.org/10.1039/d4nj02454k

‡ Juliana M. Missina and Heloísa de S. Camilo contributed equally to this article and share the first authorship.

storage,[7] and catalysis.[8] The use of POVs for the removal of dyes is less frequent, but some works show good results, mainly through photocatalytic processes. For instance, the hexavanadate $[\{Mn(salen)(H_2O)\}_6V_6O_{18}]$, where salen^{2-} = *N*,*N*′-(ethylene)bis(salicylideneiminate), was able to remove RB up to about 75% after UV irradiation for 90 min, showing better results than sodium decavanadate and $[Mn(salen)(H_2O)]$.[9] Another POV, $[V_{10}O_{16}(OH)_6(CH_3CH_2COO)_6]^{2-}$, a mixed-valence decavanadate functionalized with propionate ligands, showed photocatalytic activity for MB degradation, reaching 93% discoloration after 45 min of UV exposure.[10] Recently, $[Cu(en)_2]_4V_{18}O_{42}(H_2O)\cdot 6H_2O$ (en = ethylenediamine) showed excellent photocatalytic activity for the degradation of MB and RB.[11]

Decavanadate, $[H_xV_{10}O_{28}]^{(6-x)-}$ (x = 0 to 3) or simply V_{10}, in turn, is one of the most studied POVs. V_{10} is the thermodynamically stable vanadate form in aqueous solution at pH from 3.0 to 6.0.[12] There are hundreds of V_{10} salts described in the literature, mainly composed of three types: purely inorganic decavanadate salts,[13] decavanadate salts with cations made up of metal complexes with organic ligands,[14] and decavanadate salts with purely organic cations.[15]

Among the latter, the organic species very often display a nitrogen atom that is basic in the pH range in which V_{10} is formed, such as amino groups, pyridine and imidazole rings. Recently, the 2-aminopyridine-containing salt of V_{10} $[2\text{-ampH}]_6[V_{10}O_{28}]$ was described as capable of bleaching MB solutions through a mechanism involving cation exchange between the salt and the dye solution.[16] In our previous work, $[Cu(OH_2)_3(2\text{-amp})]_2(trisH)_2\ [V_{10}O_{28}]\cdot 2H_2O$ (tris = tris(hydroxymethyl)aminomethane) bleached MB with an efficiency of up to 84% in 20 min, wherein the insoluble V_{10} salt was subsequently retrieved.[17]

In the past few years, we have been interested in investigating the interactions between decavanadate and large cationic organic dyes, not only because they are emergent surface water pollutants, but also due to their biological use as cell and tissue colorants and fluorescent biological markers.[18] In an effort to better understand the interaction of organic dyes with V_{10}, we have studied the direct reaction between V_{10} and MB or RB, producing decavanadate salts with MB or RB as counterions. The V_{10} salt with rhodamine B, $(RB)_4[H_2V_{10}O_{28}]\cdot 2RB\cdot 14H_2O$ was fully characterized, including by single crystal X-ray diffraction (SCXRD), and was used as a fluorescent marker to study the inhibition mechanism of V_{10} towards ABC transporters, a large class of transmembrane proteins associated with multidrug resistance to chemotherapeutics.[19] The V_{10} salt with MB, in its turn, was previously obtained as an amorphous solid and primarily characterized. This work describes the SCXRD structure of $(MB)_4(H_2V_{10}O_{28})\cdot 10.8H_2O$ (**MBV$_{10}$**) and expands these studies to include toluidine blue (TB, Chart 1), which is also a thiazine dye used in textile industries and in biological assays to stain tissues rich in DNA and RNA.[20] Moreover, a novel V_{10} salt with 2-amino-3-methylpyridinium (**2,3-ampV$_{10}$**) was synthesized and tested for the adsorption of MB, TB and RB. The **2,3-ampV$_{10}$** compound selectively adsorbed MB over RB, and promoted metachromasia of TB at pH 3. The products of the direct reaction of MB and TB with decavanadate, and particularly **MBV$_{10}$**, contributed to a better understanding of the interaction mode of cationic dyes with large polyoxidoanions.

Materials and methods

All syntheses and bleaching experiments were made using ultrapure water (conductivity lower than 0.35 μS cm^{-1} at 25 °C). Reactants $NaVO_3$ (98%, Aldrich), 2-amino-3-methylpyridine (95%, Aldrich), methylene blue (MB, 3,7-bis(dimethylamino)-phenothiazin-5-ium chloride, 97%, Aldrich), toluidine blue, (TB, (7-amino-8-methylphenothiazin-3-ylidene)-dimethylammonium chloride, >85%, Merck) and rhodamine B (RB, 9-(2-carboxyphenyl)-6-(diethylamino)-*N*,*N*-diethyl-3*H*-xanthen-3-iminium chloride, 90%, Merck) were all used as received, without further purification. Vanadium contents were measured by titration according to the literature[21] or by thermal decomposition, treating samples at 550 °C to obtain V_2O_5. Elemental analyses (C, H, N) were determined by combustion in a Perkin Elmer 2400 Series elemental analyzer. The crystalline phase purity of all products was investigated by powder X-ray diffraction (PXRD) using a Shimadzu XRD-6000 diffractometer equipped with Cu-Kα radiation (λ = 1.5418 Å) in a 2θ range of 5–80°, at room temperature, with applied voltage and current of 40 kV and 30 mA. The calculated PXRD patterns were obtained using the Mercury software[22] from the data in the CIF files. Infrared spectra (IR) were obtained from KBr pellets in a VERTEX 70v spectrophotometer, with a resolution of 2 cm^{-1} within the range of 400 to 4000 cm^{-1}. The reflectance spectra of solids and the electronic spectra of the solutions resulting from the bleaching reactions were obtained in a Perkin Elmer Lambda 1050 UV-vis-NIR spectrophotometer. The scanning electron microscopy (SEM) analyses were carried out in a TESCAN VEGA3 LMU equipment at different magnifications, with a resolution of 3 nm. Energy dispersive spectroscopy (EDS) data were obtained using a chemical analysis system (Oxford) with AZ Tech software (advanced) with 80 mm^2 SDD type detector. The mass spectrum (electrospray ionization mass spectrometry, ESI-MS) was obtained using a Thermo Scientific LTQ XL™ linear ion trap mass spectrometer.

Synthesis of $(2,3\text{-ampH})_6[V_{10}O_{28}]\cdot 4H_2O$ (2,3-ampV$_{10}$)

$NaVO_3$ (0.610 g, 5.00 mmol) was solubilized in boiling water (20 mL) under stirring. The pH of the resulting colorless solution was adjusted to 4.0 using diluted HCl, giving an orange solution. A 10 mL aqueous solution of 2-amino-3-methylpyridine (302 μL, 3.0 mmol) was slowly dropped onto the decavanadate solution at room temperature (rt). The system was stored at rt and crystals suitable for SCXRD analysis were obtained after 24 h. These crystals were washed three times with cold water and dried in air. The solid was soluble in dimethyl sulfoxide, insoluble in water at pH 6, and poorly soluble in water at pH 3. Yield: 0.223g, 38% based on vanadium ($C_{36}H_{62}N_{12}O_{32}V_{10}$). IR (KBr, cm^{-1}): 3551(br), 3356(br), 3176(br), 1653(s), 1566(w), 1470(m), 1387(w), 1362(w), 1304(m), 1252(w), 947(s), 839(s), 737(m), 594(m), 538(m), 453(w). Elemental analysis (% m/m): calculated for $C_{36}H_{62}N_{12}O_{32}V_{10}$: C, 25.67; H,

3.71; N, 9.98; V, 30.24. Found for **2,3-ampV$_{10}$**: C, 25.81; H, 3.57; N, 9.88, V, 29.4.

Direct reactions between decavanadate and the organic dyes MB and TB

General method. A suspension of $NaVO_3$ (0.610 g, 5.00 mmol) in 20 mL of water was stirred at 100 °C until complete dissolution. The resulting colorless solution had its pH adjusted to 4.0 with diluted HCl, giving an orange solution characteristic of decavanadate. This solution received the dropwise addition of 10 mL of aqueous solutions of the desired organic dye (MB: 0.096 g, 0.300 mmol, or TB: 0.027 g, 0.100 mmol) at rt, and the resulting reaction mixtures were left on the bench for 24 h. The solids formed were filtered under vacuum, washed 5 times with 2 mL of cold water (4 °C) and dried in air.

MBV$_{10}$. 0.203 g of a dark green solid; yield: 17% based on vanadium. IR (KBr, cm^{-1}): 3431(br), 3348(br), 1599(s), 1489(m), 1441(w), 1392(s), 1356(s), 1252(m), 1221(m), 1178(m), 1153(m), 1040(w), 964(s), 887(s), 831(s), 760(w), 669(w), 607(w), 538(w), 451(w). Elemental analysis (% m/m): calculated for $(MB)_4[H_2V_{10}O_{28}]\cdot 13H_2O$, $C_{64}H_{100}N_{12}S_4O_{41}V_{10}$: C, 32.97; H, 4.32; N, 7.21; V 21.85. Found for **MBV$_{10}$**: C, 32.6; H, 3.92; N, 7.03; V 21.6.

TBV$_{10}$. 0.0611 g of a dark blue solid; yield: 6.5% based on vanadium. IR (KBr, cm^{-1}): 3312(br), 3182(br), 1640(m), 1599(s), 1520(w), 1489(m), 1441(m), 1383(s), 1325(s), 1238(m), 1176(m), 1138(m), 1024(w), 959(s), 878(w), 827(s), 744(m), 663(w), 596(m), 447(w). Elemental analysis (% m/m): calculated for $(TB)_4(H_2V_{10}O_{28})\cdot 10H_2O$, $C_{60}H_{84}N_{12}S_4V_{10}O_{38}$: C, 32.48; H, 3.82; N, 7.57; V, 22.96. Found for **TBV$_{10}$**: C, 32.7.; H, 3.53; N, 7.52; V, 21.6.

Single crystal X-ray diffraction analysis (SCXRD)

A single crystal of each decavanadate salt was analyzed in a Bruker D8 Venture diffractometer equipped with a Photon 100 CMOS detector. Mo-Kα radiation and a graphite monochromator were used for the analysis and intensity data were measured through thin slices ω and ϕ scans. Data processing was performed employing the APEX3[23] program. The structures were determined through the intrinsic phase routines on SHELXT[24] and refined using the full matrix least squares method on F^2's on SHELXL.[24] The crystallographic data and refinement parameters of **2,3-ampV$_{10}$** and **MBV$_{10}$** are listed in Table 1.

2,3-ampV$_{10}$. Non-hydrogen atoms, with the exception of those of one 2-amino-3-methylpyridinium cation that is affected by disorder (see below), were refined using anisotropic thermal parameters. Scattering factors for neutral atoms were taken from the literature.[25] The disorder affecting one 2-amino-3-methylpyridinium cation was refined by using two models (occupancy factors were refined to the following values: 0.84 and 0.16 for the A, and B models). In the asymmetric unit there are two disordered water molecules, these molecules were not introduced in the refinement that was carried out by using the squeeze routine in Platon. All hydrogen atoms, with the exception of those belonging to the disordered 2-amino-3-methylpyridinium cation, were found in the Fourier density map (for these atoms DFIX and DANG instructions were used during the refinement). The hydrogen atoms of the disordered cation were put in calculated positions.

MBV$_{10}$. Single crystals of **MBV$_{10}$** were obtained from a synthetic procedure similar to that described to prepare the **MBV$_{10}$** powder sample, but diluted 10 times. A lot of crystals were tested and the data reported in the present article are those obtained by the best single crystal we were able to find. Non-hydrogen atoms were refined using anisotropic thermal parameters. Scattering factors for neutral atoms were taken from the literature.[25] All hydrogen atoms of the MB cations were put in calculated positions and refined in accordance with the atom to which they are bonded. Finally, the hydrogen atom that protonates the V_{10} anion and those of the water molecules that were not found in the Fourier density maps were not introduced in the refinement.

Theoretical calculations (computational details)

Quantum chemistry calculations were performed using the density functional theory (DFT) computational method, employing

Table 1 Crystallographic data and refinement parameters **2,3-ampV10** and **MBV$_{10}$**

	2,3-ampV$_{10}$	**MBV$_{10}$**
Molecular formula	$V_{10}O_{28}$, 6($C_6H_9N_2$), 4(H_2O)	$H_2V_{10}O_{28}$, 4($C_{16}H_{18}N_3S$), 10.8(H_2O)
Molar mass (g mol^{-1})	1684.37	1155.58
Crystal system, space group	Monoclinic, $P2_1/c$	Triclinic, $P\bar{1}$
Cell parameters (Å, °)	a = 8.8451(5)	a = 12.191(2), α = 90.970(6)
	b = 15.2198(8), β = 93.605(2)	b = 13.129(3), β = 101.144(6)
	c = 21.2242(13)	c = 15.478(3), γ = 108.890(6)
Volume (Å^3)	2851.6(3)	2291.3(8)
Z	2	2
T (K)	100	300
λ (Å)	0.71073	0.71073
Density (mg m^{-3})	1.962	1.675
F(000)	1696	1178
Absorption coefficient (mm^{-1})	1.664	1.155
Crystal dimensions (mm)	0.463 × 0.080 × 0.068	0.363 × 0.116 × 0.034
Theta range for data collection (°)	2.7 to 28.3	2.5 to 21.4
Reflections collected/unique/R_{int}	230611/7083/0.0694	40861/5174/0.113
Data/parameters/restrains	7083/434/40	5174/604/0
Goodness-of-fit on F^2	1.161	1.048
Final R indices ($I > 2\sigma(I)$)	R_1 = 0.0508, wR_2 = 0.1273	R_1 = 0.0559, wR_2 = 0.1441
Final R índices (all data)	R_1 = 0.0644, wR_2 = 0.1351	R_1 = 0.0957, wR_2 = 01638

the X3LYP[26] functional and the def2-TZVP basis set,[27] as implemented in Orca 5.0.4 quantum chemistry package.[28,29] The resolution of identity approximation was used for the Coulomb part of the two electron integrals employing the def2/j auxiliary basis set, in order to accelerate the calculations. The solvent effect was modelled using the SMD solvent model.[30] Electronic transitions and absorption spectra were calculated using the path integral approach.[31–33] For this, the crystallographic geometries with optimized hydrogens were used for the ground state Hessian calculation, while, for the excited state, we employed the time dependent density functional theory (TDDFT) with the Tamm–Dancoff approximation[34] (searching through 5 roots) to determine the first ES and the Adiabatic Hessian after the step (AHAS)[33] approximation to determine its Hessian.

Reactions for the bleaching of the organic dyes

The experiments were conducted following the procedure described in the literature.[17] In a typical experiment, 10.0 mg (6.0 μmol) of **2,3-ampV$_{10}$** were directly added to 50 mL of a 10 mg L^{-1} aqueous solution of MB, TB or RB at rt under magnetic stirring. The reactions were conducted at the initial pH of the dye solutions (6.2–6.5), and at pH 3.0 (pH adjusted with HCl, 0.10 mol L^{-1}) 16 and 4.0 mg of **2,3-ampV10** were also used for TB, following the same procedure described above. Aliquots of 4.0 mL of the reaction media were taken at 2, 5, 10, and 15 min after the start of the reactions. Each aliquot was centrifuged at 8000 rpm for 1 min and the supernatant was carefully removed for subsequent UV-vis analysis, monitoring the intensity of the band at 664 nm (MB), 630 nm (TB) and 554 nm (RB). For MB, amounts of 1, 2, and 4 mg of **2,3-ampV10** were also tested, whereas the bleaching capacity of **2,3-ampV10** towards each dye was calculated using the formula % = $(A_0 - A)/A_0 \times 100$, wherein A_0 is the absorbance of the dye solution before the reaction and A is the absorbance of the reaction solution at any time point. All experiments were run at least in triplicate, and the results are expressed as arithmetic averages, considering mean ± standard deviation (SD).

Results and discussion

Characterization of 2,3-ampV$_{10}$ by SCXRD

The reaction of decavanadate with 2-amino-3-methylpyridine in aqueous solution produced yellow crystals suitable for SCXRD. The elemental analysis (data are shown in the experimental section) and the comparison between simulated and experimental PXRD patterns (Fig. S1, ESI†) confirm the crystalline purity of the sample. **2,3-ampV$_{10}$** crystallizes in the monoclinic crystal system, $P2_1/c$ space group. The asymmetric unit contains three 2,3-ampH$^+$ cations, half a completely deprotonated $[V_{10}O_{28}]^{6-}$ anion and two disordered water molecules; hence, the compound can be formulated as $(2,3\text{-ampH})_6[V_{10}O_{28}]\cdot 4H_2O$ (Fig. 1 and Fig. S2, ESI†). The decavanadate anion in **2,3-ampV$_{10}$**, as well as in **MBV$_{10}$**, consists of 10 edge-sharing distorted VO_6 octahedra. Selected bond lengths and angles are reported in Table S1 (ESI†) and are in accordance with

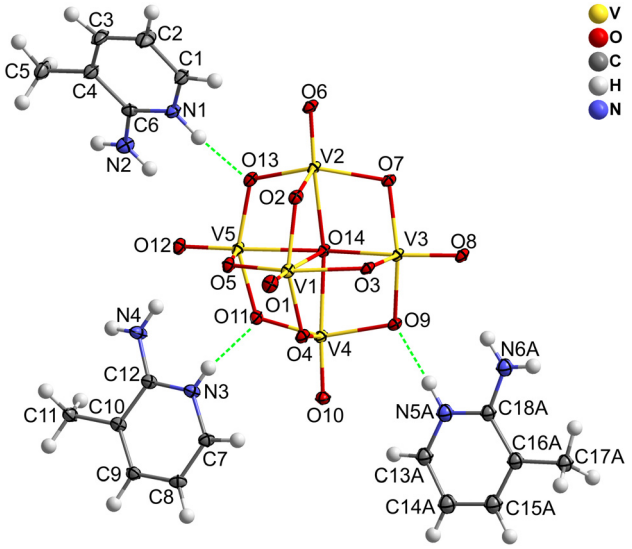

Fig. 1 Asymmetric unit of **2,3-ampV$_{10}$**. Ellipsoids have been drawn at 30% probability. Hydrogen atoms are represented as spheres with fixed radius of 0.2 Å. Just one model (the one with the biggest occupancy factor) for the (N5, N6) 2-amino-3-methylpyridinium cation has been reported.

those found in the literature.[35] The bond lengths increase in the order V=O < V–μ_2-O < V–μ_3-O < V–μ_6-O.

The 2-amino-3-methylpyridinium cations are organized in trimers, with the pyridine rings involved in π–π interactions (Fig. 2A), with distances between centroids of 3.556(7) and 3.595(8) Å (Table 2), which fall within the expected range for this type of interaction.[36]

The trimers are disposed along the *c* axis forming a chain (Fig. 2B), with a distance between consecutive trimers of about 4.31 Å (Table 2).

A net of hydrogen bonds links the 2,3-ampH$^+$ cations to the V_{10} anions; as expected, the strongest hydrogen bonds involve the protonated pyridine nitrogen atoms (N1, N3 and N5) and the most basic oxygen atoms of decavanadate, *i.e.*, μ_3-O (O9) and μ_2-O (O11, O13). One of the three 2,3-ampH$^+$ cations (the one containing the nitrogen atoms N5 and N6) interacts with just one V_{10}, while the other cations connect two adjacent V_{10}, thus forming a unidimensional chain that extends along the *a* axis (Fig. 2C and Table 3). Finally, these chains are held together by the 2-amino-3-methylpyridinium trimers (Fig. S2, ESI†). The net of interactions involving the 2,3-ampH$^+$ and the V_{10} anions gives rise to the formation of isolated pockets where the water molecules are located (Fig. 2C). The voids were calculated using the Mercury software[22] with a probe radius of 1.2 Å and approx. grid spacings of 0.7 Å, leading to a volume of 7.2% of the unit cell.

Aminopyridines have been largely employed as cations to V_{10} in diverse salts, either alone or as ligands to other metals in cationic complexes. Table S2 (ESI†) gathers the V_{10} salts with aminopyridines found in a recent search in the CCDC database.[16,37–46] Among them, 7 are alkylaminopiridinium salts, wherein the structures of $[3\text{-ampH}]_6[V_{10}O_{28}]\cdot 2H_2O$ (3-ampH = 3-aminopyridinium),[42] $[4\text{-dmampH}]_6[V_{10}O_{28}]\cdot 16H_2O$[44,45] and $[4\text{-dmampH}]_4(NH_4)_2[V_{10}O_{28}]\cdot 8H_2O$[46]

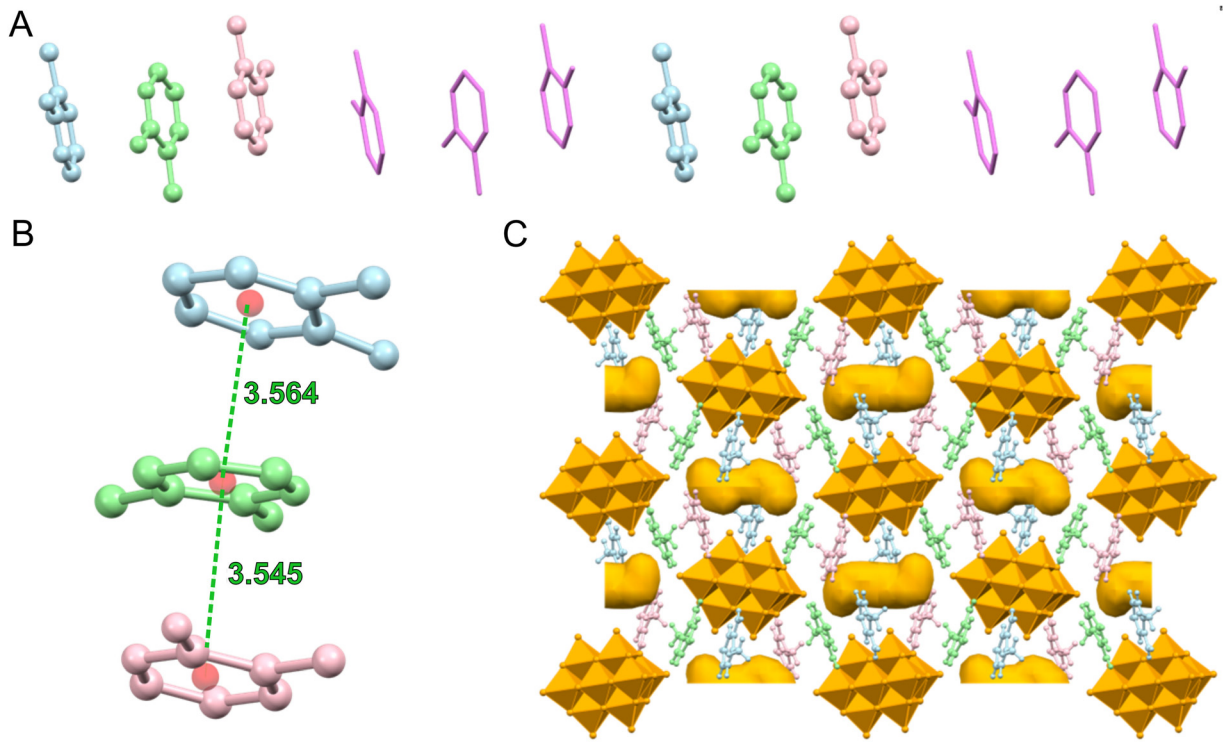

Fig. 2 (A) 2-Amino-3-methylpyridinium cation trimers viewed along the *a* axis (pink: the cation containing the N1 and N2 nitrogen atoms, light green: the cation containing the N3 and N4 nitrogen atoms, pale blue: the cation containing the N5 and N6 nitrogen atoms). (B) Disposition of the 2,3-ampH$^+$ trimers along the *c* axis. (C) Crystal packing of **2,3-ampV$_{10}$** (with, in orange, the voids where the water molecules are located).

Table 2 Selected distances between centroids and angles between planes in **2,3-ampV$_{10}$** and **MBV$_{10}$**

2,3-ampV$_{10}$

Distances (Å) between centroids of the pyridine rings and angles (°) between the mean plane containing the pyridine fragment (the moieties are identified by the nitrogen atoms)

	Distance (Å)	Angle (°)
(N1, N2)/(N3, N4)[a]	3.545(6)	15.1(1)
(N3, N4)/(N5, N6)[b]	3.443(7)/3.801(4)	6.1(2)/7.2(3)
(N1, N2)/(N5, N6)[c]	4.310(5)/4.065(6)	28.2(3)/29.1(3)

MBV$_{10}$

Distances (Å) between centroids of the 1,4-thiazine rings and angles (°) between the mean plane containing the MB cations (the moieties are identified by the sulfur atom)

	Distance (Å)	Angle (°)
S1/S2	3.805(2)	5.2(2)
S1/S1[d]	3.876(2)	0
S2/S2	3.726(2)	0

[a] 2 − *x*, −0. + −*y*, 1.5 − *z*. [b] 1 + *x*, *y*, *z*. [c] 1 − *x*, 1 − *y*, 1 − *z*. [d] 1 − *x*, −*y*, 1 − *z*.

Table 3 Selected intermolecular interactions in **2,3-ampV$_{10}$**

X–H···Y	X···Y (Å)	H···Y (Å)	X–H···Y (°)
V$_{10}$ anions···water molecules interactions[a]			
O1w···O1	2.85(2)/2.86(2)/2.79(3)		
O1w···O10[c]	3.11(2)/3.27(2)/3.44(3)		
O2w···O6[d]	2.89(3)/2.94(2)/2.92(3)		
V$_{10}$ anions···2,3-ampH$^+$ cations interactions			
N4–H3b···O4	2.960(6)	2.146(3)	157.8(3)
N5–H5···O9	2.733(6)	1.882(3)	170.0(4)
N6–H6a···O8	3.193(7)	2.378(3)	158.3(4)
N2–H2a···O12[d]	3.044(6)	2.313(4)	143.1(4)
N1–H1a···O13[d]	2.682(6)	1.844(3)	164.4(3)
N3–H3a···O11[e]	2.671(5)	1.818(4)	171.1(3)
N4–H4a···O12[e]	3.004(6)	2.207(4)	154.2(4)
N2–H2b···O2[f]	2.879(6)	2.081(3)	154.1(3)
N6–H6b···O7[g]	3.153(7)	2.311(3)	166.1(4)
Water molecules interactions			
O1w···O2w	2.57(4)–2.90(4)[b]		
O2w···O2w[h]	2.52(4)–3.02(4)[b]		

[a] Where three values are reported they refer to the three models of water molecules used during the refinement. [b] The range of the retrieved distances between water molecules oxygen atoms is reported. [c] 1 − *x*, −0.5 + *y*, 1.5 − *z*. [d] 1 − *x*, 0.5 + *y*, 1.5 − *z*. [e] −1 + *x*, *y*, *z*. [f] −*x*, 0.5 + *y*, 1.5 − *z*. [g] −*x*, 1 − *y*, 1 − *z*. [h] 1 − *x*, 1 − *y*, 2 − *z*.

(dmampH = 4-(*N*,*N*-(dimethylamino)pyridinium)) present comparable π–π interaction distances that define the pattern of the cations. In addition, a similar pattern was found in [2-ampymH]$_6$[V$_{10}$O$_{28}$]·5H$_2$O (ampymH = 2-aminopyrimidinium).[36]

Reactions between decavanadate and cationic organic dyes in aqueous solution

The direct reactions of V$_{10}$ with MB and TB in aqueous solution immediately gave precipitates due to the high negative charge and oxygen-rich surface of the decavanadate anion. The SEM

images from these solids provided further information about the microstructure and morphology of **MBV$_{10}$** and **TBV$_{10}$** salts, and these solids were compared with the crystals obtained from the reaction that gave product **2,3-ampV$_{10}$** (Fig. 3A–C). Upon examination of these SEM images, it was observed that the crystallinity and surface properties of the products change depending on the nature of the countercation. While **2,3-ampV$_{10}$** is crystalline, the reactions with the dyes gave pure homogeneous microcrystalline **MBV$_{10}$**, and amorphous **TBV$_{10}$** solids. The elemental analyses of both products suggested similar formulations, with four cationic dyes for each V_{10}, $(MB)_4[H_2V_{10}O_{28}]\cdot 13H_2O$ for **MBV$_{10}$**, and $(TB)_4[H_2V_{10}O_{28}]\cdot 10H_2O$ for **TBV$_{10}$**, differing only in the number of water molecules. The EDS analysis is a semiquantitative method that can be performed concomitantly with the SEM imaging of the samples. For all products, elemental percentages close to the ones expected were found (Fig. 3).

Attempts to produce crystalline products were performed by slow diffusion of highly dilute aqueous solutions of the selected dyes to the V_{10} reaction mixture. However, even after several attempts, we were capable to grow only few amounts of fragile bright green single crystals of **MBV$_{10}$**. PXRD analysis of this product batch revealed good correspondence between the calculated and experimental diffraction patterns (Fig. S3, ESI†). The partial differences in relative intensities might be due to the preferred orientation of the crystallites in the powdered sample. Unfortunately, none of the synthetic approaches attempted produced crystalline samples of **TBV$_{10}$**, even in highly diluted reaction media. As expected, the PXRD pattern showed low crystallinity, presenting broad peaks at 3.5, 9.5, 26, 43 and 65° 2θ (Fig. S4, ESI†).

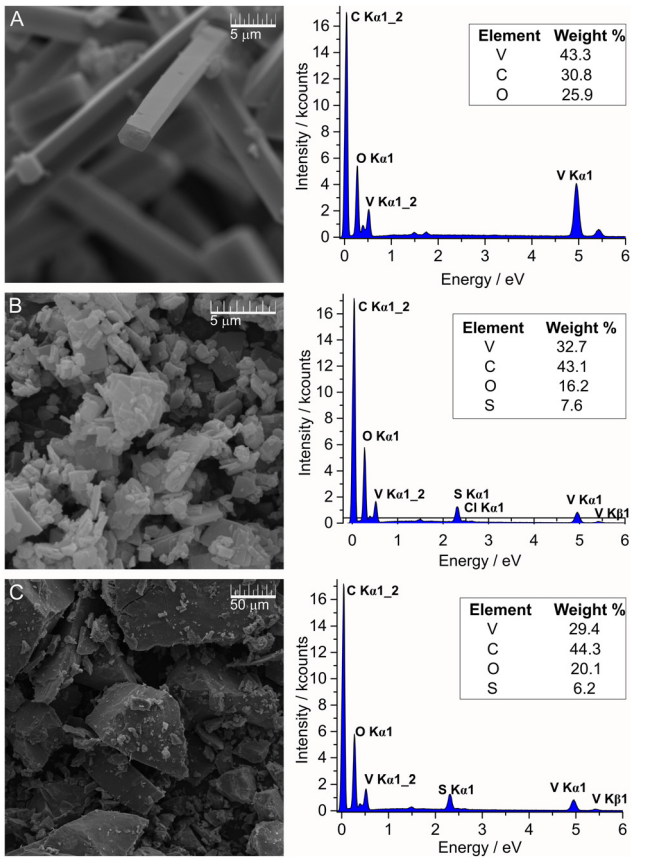

Fig. 3 Scanning electron microscopy (SEM) images at different magnifications (left) and EDS spectra (right) of: (A) crystalline **2,3-ampV$_{10}$** × 10 000, (B) microcrystalline solid obtained from the direct reaction of an aqueous decavanadate solution with methylene blue (**MBV$_{10}$**) × 15 000 and (C) amorphous solid obtained from the mixture of an aqueous decavanadate solution with toluidine blue (**TBV$_{10}$**) × 1000.

Infrared spectroscopy (IR)

The IR spectra of **2,3-ampV$_{10}$**, **MBV$_{10}$** and **TBV$_{10}$** (Fig. S5–S7 and Tables S3 and S4, ESI†) display typical decavanadate anion bands[47] at 947–964 cm^{-1}, 827–839 cm^{-1}, 737–760 cm^{-1}, and 594–663 cm^{-1} assigned to ν(V=O), ν_{as}(V–O), ν_{as}(V–O) and δ(V–O–V), respectively.

Broad bands in the region of 3200 to 3500 cm^{-1} are attributed to ν(O–H) of the water molecules.[48] The spectral profiles differ from each other due to the cations that balance the charge of V_{10}. The spectrum of **2,3-ampV$_{10}$** shows a band related to the $\nu(C–C)_{ring}$ of 2,3-ampH$^+$ at 1653 cm^{-1} and vibrations expected for the pyridine ring at 1252, 839, 737, and 538 cm^{-1}.[49] For **MBV$_{10}$** and **TBV$_{10}$**, the region between 1000 and 1600 cm^{-1} presents bands of ν(C–S–C) at 1040 and 1025 cm^{-1}, ν(C=S$^+$) at 1489 and 1486 cm^{-1}, and ν(C=N) at 1599 and 1600 cm^{-1}, referring to vibrational modes of the thiazine rings.[50,51]

Characterization of MBV$_{10}$ by SCXRD analysis

Despite the well-formed appearance of the **MBV$_{10}$** crystals, they don't diffract very well, even at low temperature, thus impairing the completeness of data. Hence, the crystal structure reported here corresponds to the best set of data from several attempts of syntheses at different dilutions. The **MBV$_{10}$** crystal belongs in the triclinic space group, $P\bar{1}$ crystal system. In the asymmetric unit two methylene blue cations and half a doubly protonated decavanadate anion are present. In addition, several water molecules (with a global occupancy factor of 5.4) are present, giving the formula $[MB]_4[H_2V_{10}O_{28}]\cdot 10.8H_2O$ (Fig. 4 and Fig. S8, ESI†), which differs in 2.2 water molecules from that proposed for the bulk sample considering the elemental analysis data. The protonation hydrogen atoms of the anion $[H_2V_{10}O_{28}]^{4-}$ were not found in the Fourier density map and were not introduced in the refinement. Finally, the V_{10} anion and the MB cations present bond lengths and angles in accordance with those found in the literature.[46,52]

The MB cations, due to the presence of π–π stacking interactions between their aromatic rings, are organized in columns propagating along the *ab* plane bisector (Fig. 5A). The monomers of the non-alternated dimer (S1/S2) are displaced by 5.2°, while the two similar alternated face-to-face dimers (S1/S1 and S2/S2) differ in the distance between centroids (Table 2). To better visualize these dimers see Fig. 6A.

These MB columns are connected by H-bond interactions with V_{10} anions (Table 4), and the resulting crystal packing shows the presence of channels (Fig. 5C and D) where all water

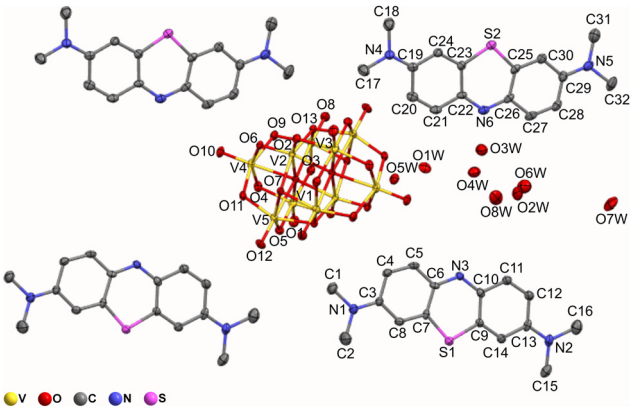

Fig. 4 Ellipsoid representation of $[MB]_4[H_2V_{10}O_{28}]\cdot 10.8H_2O$. Ellipsoids have been drawn at 30% probability. Hydrogen atoms of the MB cations have been omitted for clarity.

molecules are located, except for O5w (occupancy factor = 0.8) and O7w (occupancy factor = 0.6).

The structure of **MBV_{10}** is similar to the Keggin-type polyoxidometalate $[MB]_4[PMo_{12}O_{40}]\cdot 2dmf\cdot H_2O$ (structure not reported on the CCDC databank)[53] but differs from those reported for the Lindqvist-type $MB_2[Mo_6O_{19}]\cdot 2dmf$ (CCDC refcode IMIROM) and $MB_2[W_6O_{19}]\cdot 2dmf$ (CCDC refcode IMIRIG).[54]

The chemical nature of the anionic counterpart and the presence of other species in the framework, especially water molecules, alongside the possibility of π–π stacking interactions between MB cations seem to determine a range of different MB aggregates reported in the literature.[53,54]

Absorption spectrum of MBV_{10} and theoretical calculations

The diffuse reflectance spectrum of **MBV_{10}** (Fig. 6) in the visible region shows an asymmetric broadband with a maximum at 664 nm ascribed to the π→π* transition of MB cations[55] and a shoulder that extends to near-infrared wavelength.

To further rationalize the contribution of MB aggregation, we calculated the electronic absorption spectra for the MB monomer and for the different dimers found in the crystallographic structure (Fig. 6A), excluding V_{10} and the water molecules,

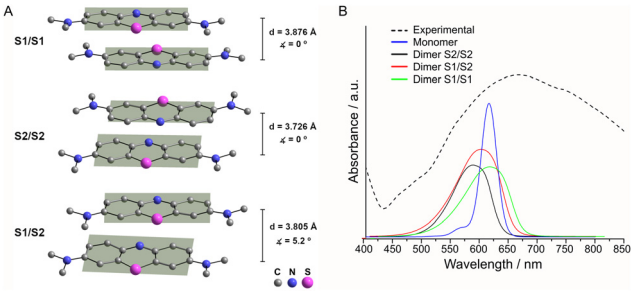

Fig. 6 (A) Representation of the dimers in the MB columns. (B) Diffuse reflectance spectrum of **MBV_{10}** (dashed) and calculated absorption spectra for the MB monomer and for the dimers at the X3LYP/Def2-TZVP/SMD theory level.

Table 4 Selected[a] intermolecular interactions in **MBV_{10}**

X–H···Y[b] MB cations ··· V_{10} anions	X···Y (Å)	H···Y (Å)	X–H···Y (°)
C4–H4···O9	3.30(1)	2.397(6)	164.4(5)
C15–H15b···O4[c]	3.60(1)	2.683(6)	158.9(7)
C2–H2a···O8[d]	3.21(1)	2.251(6)	176.1(7)
C1–H1a···O8[d]	3.50(1)	2.585(7)	158.4(6)
C1–H1c···O13[e]	3.66(1)	2.779(5)	153(7)
C28–H28···O2[e]	3.66(1)	2.784(5)	156.4(6)
C20–H20···O5[f]	3.40(1)	2.566(6)	150.1(6)
C12–H12···O12[f]	3.22(1)	2.328(7)	161.3(6)
C17–H17a···O1[g]	3.34(1)	2.385(6)	170.4(6)
C18–H18a···O1[g]	3.50(1)	2.578(6)	161.2(6)

[a] H···O distance shorter than 2.8 Å, C–H···O angle larger than 150. [b] Carbon atoms from C1 to C16 belong to the MB cation containing S1, carbon atoms from C17 to C32 belong to the MB cation containing S2. [c] $-x, 1-y, 1-z$. [d] $-x, 1-y, 2-z$. [e] $1-x, 1-y, 2-z$. [f] $1-x, 1-y, 1-z$. [g] $x, 1+y, -1+z$.

applying a molecular modelling based on DFT.[33] The theoretical absorption spectra for the S2/S2 and S1/S2 dimers, when compared to the monomer one, present a hypsochromic shift (Fig. 6B), which is in accordance with other experimental and theoretical studies.[56–58] In contrast, the S1/S1 dimer shows a bathochromic shift, leading to a possible correlation of the

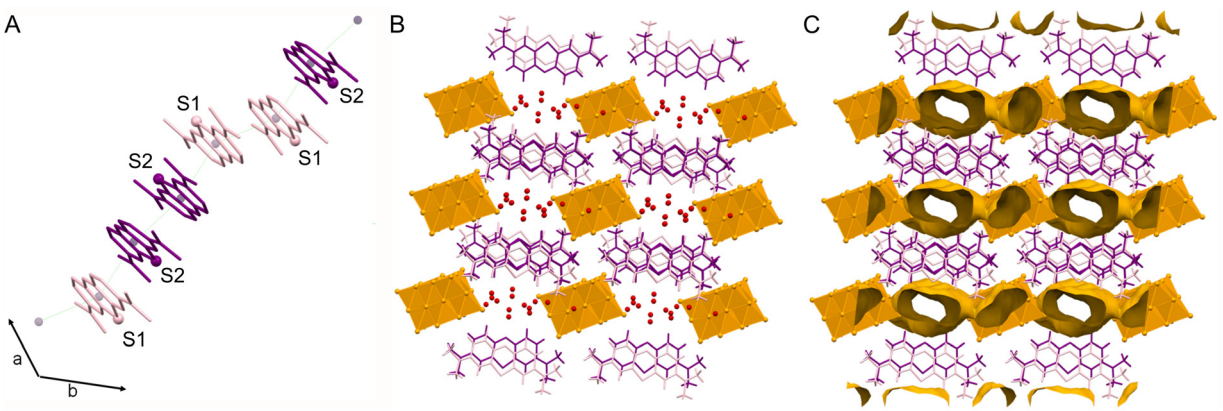

Fig. 5 (A) MB column along the *c* axis (B) crystal packing of **MBV_{10}**, (C) voids in the crystal packing of **MBV_{10}** (voids were calculated with the "voids" routine in mercury, probe radius = 1.2 Å, approx. grid spacings = 0.7 Å, voids are 19% of the unit cell volume).

distances between the monomers in the dimers with the band shift. Additionally, in MB aggregates, cations experience non-bonding interactions that shift transition dipole moments and broaden the electronic spectra.[58] As reported for $[N\mathrm{Bu}_4]_2[\mathrm{M}_6\mathrm{O}_{19}]$, M = $\mathrm{Mo}^{\mathrm{VI}}$, W^{VI},[54] $[\mathrm{MB}]_4[\mathrm{PMo}_{12}\mathrm{O}_{40}]$ and $[\mathrm{MB}]_4[\mathrm{GeMo}_{12}\mathrm{O}_{40}]$,[53] charge transfer transitions between the MB donor and the polyoxidoanion acceptor, excluded in the calculations, could be responsible for the presence of the shoulder that extends this band to over 850 nm.

Studies of the discoloration of organic dyes using 2,3-ampV$_{10}$

The studies were initiated by the immersion of 10.0 mg of **2,3-ampV$_{10}$** in aqueous solutions of each dye (MB, TB and RB) at 10.0 mg L^{-1} under continuous magnetic stirring, monitoring the absorbance of MB (664 nm), RB (554 nm) and TB (630 nm) over time. For MB, a discoloration of 85% was reached after only 2 min, achieving a maximum of 90% at 15 min (Fig. 7A), whereas solutions of RB were barely discolored after up to 4 h (see Fig. S9, ESI†). Given the high efficacy of **2,3-ampV$_{10}$**, decreasing amounts of the compound were tested (Fig. 7D). Even as little as 2.0 mg caused over 80% discoloration after 15 min; however, a marked decrease in bleaching to 32% was noticeable with 1.0 mg. Moreover, **2,3-ampV$_{10}$** was also tested adjusting the pH of each dye solution to 3.0 and fixing the amount of the compound at 10.0 mg. No changes were observed in the RB solution. By contrast, for MB the bleaching effect increased from 85% to 95% after 2 min (Fig. 7B and E and Table S5, ESI†).

MB is a well-known redox indicator, wherein its oxidized cationic form is blue, and its neutral form, protonated at the central thiazine nitrogen, is colorless, known as *leuco*-methylene blue (LMB).[57] LMB typically absorbs only at UV wavelengths, presenting two bands at 314 and 256 nm.[34] As depicted in Fig. 7B, the full spectra of aqueous MB solutions after reactions with **2,3-ampV$_{10}$** at pH 3.0 and 6.0 exhibit a maximum absorbance at the UV region at 296 nm, related to the π–π* transition of MB,[59] indicating that the discoloration promoted by **2,3-ampV$_{10}$** is not given by a simple redox process.

To check for any competitive or cooperative effects of the dyes, we have also tested a binary system containing 5.0 mg L^{-1} of each dye (Fig. 7C). In comparison with pure solutions, RB interferes in the interaction of MB with the V_{10} salt in the beginning of the assay, resulting in only 10% bleaching after 2 min. From 10 min onwards, a preferred removal of MB over RB was observed, starting at a ratio of *ca.* 7 : 1 and reaching a 10 : 1 ratio after 20 min of stirring (Fig. 7F). Selectivity for certain cationic dyes has been previously observed for other POMs. For example, $Cs_4H_2PMo_{11}FeO_{40}$[59] and $H\{Nd_4L_2(H_2O)_{21}[Zr_3(OH)_3(PW_9O_{34})_2]\}$, L = 3,5-(pyridine dicarboxylic acid)[60] were shown to be excellent selective adsorbents of MB when tested in an aqueous mixture of MB, RB and methyl orange, an anionic dye. Here, the preferential interaction with MB in contrast with RB might be attributed to the lower stereo hindrance of the MB cation, which has dimensions of 17 Å by 7.6 Å in a planar structure,[61] while RB is larger in size, presenting a non-planar structure, with dimensions of approximately 16 Å by 11 Å, and a freely-rotating benzoate group.[62] To investigate the bleaching capacity of **2,3-ampV$_{10}$**, another member of the thiazine family, TB (11 Å by 7 Å),[63] was also tested, starting the experiment with 10 mg L^{-1} of TB at pH 6 and pH 3 (Fig. 8A and B). The bleaching effect was lower for the TB solution at pH 6.0 than for MB, reaching a maximum of 77, 70 and 50% after 15 min using 16.0, 10.0 and 4.0 mg of **2,3-ampV$_{10}$**, respectively (Fig. 8C and D). Despite structural similarities, in TB the charge is localized on the nitrogen atom of the dimethylamine group, while in MB its C_{2v} point group symmetry indicates that its charge can be equally found on both dimethylamine groups.[59] These differences in location of the positively charged atom contribute to

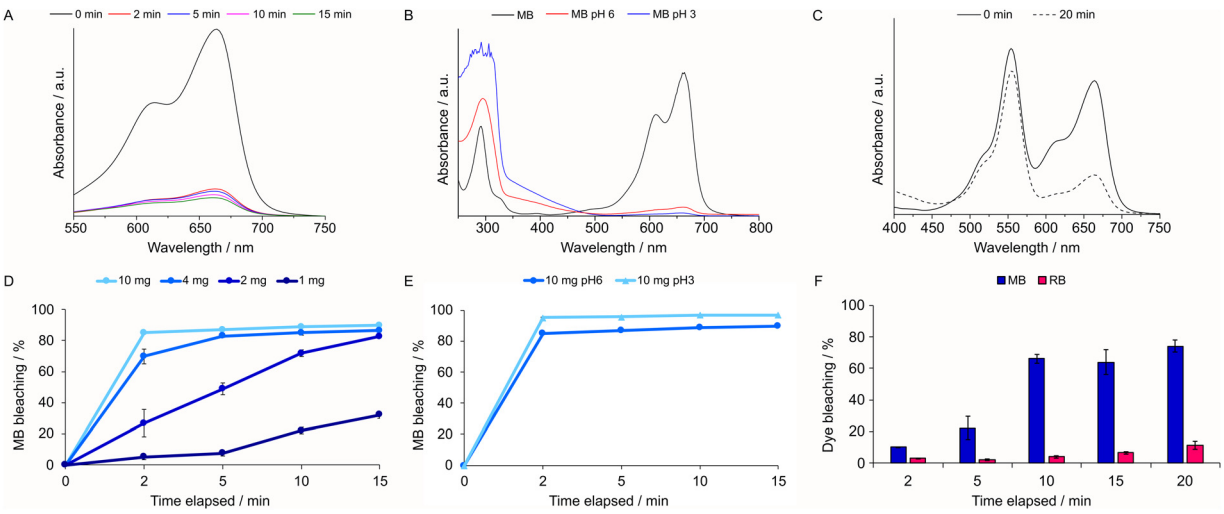

Fig. 7 Electronic spectra and bleaching assays using 50 mL of the dye solutions: (A) 10.0 mg of **2,3-ampV$_{10}$** in a 10.0 mg L^{-1} MB solution at pH 6.0; (B) 10 mg of **2,3-ampV$_{10}$** in 10 mg L^{-1} aqueous solutions of MB at pH 6 (red line) and pH 3 (blue line), as compared to the absorption spectrum of pure MB at 10 mg L^{-1} (black line); (C) 10.0 mg of **2,3-ampV$_{10}$** in a mixed solution of MB and RB at 5.0 mg L^{-1} each, at pH 6.0; (D) decreasing amounts of **2,3-ampV$_{10}$** in MB solutions at pH 6.0; (E) line plots showing the percentage of MB (10 mg L^{-1}) bleaching upon addition of **2,3-ampV$_{10}$** at two different pH in time; (F) percentage of MB and RB bleaching (5.0 mg L^{-1} each) in time.

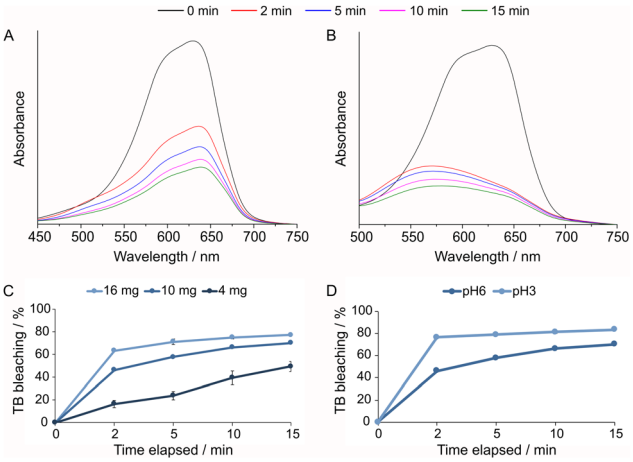

Fig. 8 Electronic spectra of the supernatants of the bleaching reactions using 10 mg of **2,3-ampV$_{10}$** in 10 mg L^{-1} aqueous solutions of toluidine blue: (A) pH 6 and (B) pH 3, indicating the absorptions of momomeric ($TB_{monomer}$ λ_{max} = 630 nm), dimeric (TB_{dimer}) and metachromatic ($TB_{methacromic}$ λ_{max} = 570 nm) forms. Line plots showing the % bleaching efficiency of (C) various amounts of **2,3-ampV$_{10}$** to aqueous solutions of TB at pH 6, and (D) at two different pH in time.

determine the interactions between each cationic dye and the V_{10} anion.[60] A noticeable change in color from dark blue to light purple was observed when the TB solution at pH 3.0 received the addition of **2,3-ampV$_{10}$**, accompanied by a hypsochromic shift from 654 nm to 570 nm (Fig. 8B).

The observed shift is related to metachromasy, a phenomenon in which aggregation of dye molecules over the surface of a material or in the presence of large anions in solution causes a shift of the absorption band.[19] A similar effect has also been described when heptamolybdate $[Mo_7O_{24}]^{6-}$ was used as complexing agent for the removal of TB by ultrafiltration.[64]

In an attempt to identify the chemical species that were present in solution, the supernatants of the reactions were analyzed by ESI-MS (Table 5). The mass spectra for the MB solution and the supernatant of the reaction with 10 mg of **2,3-ampV$_{10}$**, after 15 min, showed peaks of higher molar weight at *m*/*z* 284 (MB, $C_{16}H_{18}N_3S^+$), 270 (Azure B, $C_{15}H_{16}N_3S^+$) and 268 ($C_{15}H_{14}N_3S^+$, assigned to MB having lost a methyl group as a methane molecule) (Fig. S10, ESI†).[65]

Azure B is commonly present in MB solutions and is formed by the photooxidative demethylation of MB promoted by light. Since the maximal absorption of Azure B is at 645 nm,[66] the bleaching of the solution cannot be explained by the presence of this compound. At lower molar weight, a peak at *m*/*z* 109 ($C_6H_9N_2^+$) corresponds to 2,3-ampH$^+$.

The ESI-MS spectra of the TB solution and bleached TB (after the reaction with 10 mg of **2,3-ampV$_{10}$** for 15 min) contain peaks at *m*/*z* 284 ($C_{16}H_{18}N_3S^+$), 270 ($C_{15}H_{16}N_3S^+$), 256 ($C_{14}H_{14}N_3S^+$) and 254 ($C_{14}H_{12}N_3S^+$), that represent the species in high abundance (Fig. S11, ESI†). The molecular weight of TB is 270.37 g mol^{-1} but the presence of other compounds could be attributed to impurities within the TB sample.[67] There is also a hypothesis that demethylation compounds (indicated by the peaks at *m*/*z* 256 and 254) can occur because of oxidative

Table 5 Main species detected by ESI-MS in the supernatants of each colorant solution after reaction with **2,3-ampV$_{10}$**

Dye	Species	*m*/*z*
MB	$C_{16}H_{18}N_3S^+$ (MB)	284
	$C_{15}H_{16}N_3S^+$ (Azure B)	270
	$C_{15}H_{14}N_3S^+$	268
	$C_6H_9N_2^+$ (2,3-ampH$^+$)	109
TB	$C_{15}H_{16}N_3S^+$ (TB)	270
	$C_{14}H_{14}N_3S^+$	256
	$C_{14}H_{12}N_3S^+$	254
	$C_6H_9N_2^+$ (2,3-ampH$^+$)	109.9
	$C_6H_6N^+$	91.9

demethylation in the electrospray process.[68] The peaks at *m*/*z* 109.9 and 91.9, present in the supernatant from the reaction with **2,3-ampV$_{10}$**, correspond to the 2,3-ampH$^+$ ($C_6N_2H_9^+$) and $C_6NH_6^+$, respectively, as shown in Fig. S12 (ESI†). In summary, despite the non-quantitative character of ESI-MS, it clearly suggests that the dyes are not being degraded during the bleaching process, evidencing a cation exchange process.

The remaining solids from each discoloration reaction were analyzed by IR. For all conditions, the IR profiles show bands of the parent solid **2,3-ampV$_{10}$** and those expected for the dyes (Table S3, ESI†). When the reaction with MB was carried out at pH 6.0, there was a predominance of the bands of **2,3-ampV$_{10}$** in the retrieved solid (Fig. S6, top, ESI†). On the other hand, for the MB solution at pH 3.0, the IR profile of the remaining solid is more similar to the spectrum of **MBV$_{10}$** (Fig. S6, ESI†), suggesting a higher incorporation of the dye into the final product. As expected, this effect is less pronounced for TB, probably due to its localized charge (Fig. S7, ESI†). For this dye, the solids isolated from the reactions at pH 6.0 and 3.0 present the same IR profile that resemble that of the parent solid. In view of the exposed results, the bleaching promoted by **2,3-ampV$_{10}$** could be considered a complex process, involving at least the interaction of the dye with the material surface and cation exchanges.

Conclusions

Decavanadate-based materials have been barely explored in the treatment of water bodies contaminated with emergent pollutants. A few examples that addressed textile industries focused on methylene blue removal. Herein, a new decavanadate salt $(2,3\text{-ampH})_6[V_{10}O_{28}]\cdot 4H_2O$ was successfully synthesized and initially evaluated for its capacity to bleach MB solutions. Additional assays with RB and TB were used as model systems to explore the potential of V_{10} for the treatment of dye-contaminated wastewater. The preference for the bleaching of MB and TB in contrast to RB was attributed to the larger size and non-planar structure of the latter relative to the other dyes. For the first time, the metachromatic effect of TB involving decavanadate materials has been described and attributed to the formation of aggregates. Despite our efforts to characterize the remaining solids and supernatants by spectroscopic and mass spectrometry techniques, the bleaching mechanisms of

MB and TB solutions remain elusive. The available data pointed to the occurrence of at least two processes that could involve cation exchange and dye interactions with the surface of **2,3-ampV$_{10}$**. The direct reactions of decavanadate with the dyes gave products with similar formulas, reflecting the high affinity of V_{10} for large cations. Particularly, $(MB)_4[H_2V_{10}O_{28}]\cdot 10.8H_2O$ (**MBV$_{10}$**) has provided a set of results that contains many structural insights into the interaction between V_{10} and a cationic organic dye. In summary, the results presented in this work bring light onto the understanding of the interaction processes of dyes, not only with V_{10} but also, by analogy, with a range of large polyoxidoanions.

Author contributions

All the authors have accepted responsibility for the entire content of this submitted manuscript and approved submission. Conceptualization, J. M. M. and G. G. N.; methodology and investigation, H. S. C., R. C. R. B., I. P. S. S.; L. G. F.; P. R. and P. P.; validation, G. G. N., E. L. S. and P. R.; writing – original draft preparation, G. G. N., J. M. M., H. S. C. and P. R.; writing – review and editing, G. G. N., J. M. M. and H.S.C.; supervision, G. G. N. and E. L. S.; project administration, G. G. N.; funding acquisition, G. G. N. and E. L. S.

Data availability

The CIF files for $(MB)_4[H_2V_{10}O_{28}]\cdot 10.8H_2O$ and $(2,3\text{-ampH})_6[V_{10}O_{28}]\cdot 4H_2O$ are available from the Cambridge Crystallographic Data Centre (CCDC) (deposition numbers CCDC: 2357605 and 2357606, respectively). The authors will make other raw data supporting this article's conclusions available upon request.

Conflicts of interest

There are no conflicts to declare.

Acknowledgements

E. L. S., L. G. F. and H. S. C. are grateful to the Centro Nacional de Processamento de Alto Desempenho (CENAPAD-SP) for providing access to computational infrastructure. Authors thank the Centro de Microscopia Eletrônica (CME/UFPR) for the SEM and EDS analyses. The authors gratefully thank Dr Jaisa Fernandes Soares for the discussions and helpful suggestions. J. M. M., H. S. C., L. G. F., and G. G. N. thank CNPq, CAPES-PrInt (Finance Code 001) and pesquisa/PRPPG/UFPR for research grants and scholarships. This study was academically funded by government agencies with no private resources. This work was financially supported by the Conselho Nacional de Desenvolvimento Científico e Tecnológico (CNPq, Project No. 406946/2021-3; 309691/2021-4), Coordenação de Aperfeiçoamento de Pessoal de Nível Superior (CAPES), Programa Institucional de Internacionalização da CAPES (CAPES—PrInt), pesquisa/PRPPG/UFPR (04/2023) and Universidade Federal do Paraná (UFPR).

Notes and references

1 A. Garg and L. Chopra, *Mater. Today: Proc.*, 2022, **48**, 1310–1315.
2 P. Dedetemo Kimilita, Y. Yoshimi and N. Sonoyama, *ACS Appl. Energy Mater.*, 2024, **7**, 629–638.
3 B. D'Cruz, M. O. Amin and E. Al-Hetlani, *Ind. Eng. Chem. Res.*, 2021, **60**, 10960–10977.
4 C. Sabarinathan, P. Karuppasamy, C. T. Vijayakumar and T. Arumuganathan, *Microchem. J.*, 2019, **146**, 315–326.
5 M. Aureliano, N. I. Gumerova, G. Sciortino, E. Garribba, A. Rompel and D. C. Crans, *Coord. Chem. Rev.*, 2021, **447**, 214143.
6 K. Szałowski, *J. Magn. Magn. Mater.*, 2022, **546**, 168782.
7 T. Zhou, L.-L. Xie, Y. Niu, H.-R. Xiao, Y.-J. Li, Q. Han, X.-J. Qiu, X.-L. Yang, X.-Y. Wu, L.-M. Zhu, H. Pang and X.-Y. Cao, *Rare Met.*, 2023, **42**, 1431–1445.
8 J. Li, C. Wei, Y. Han and C. Hu, *Dalton Trans.*, 2023, **52**, 12582–12596.
9 Q. Wu, X. Hao, X. Feng, Y. Wang, Y. Li, E. Wang, X. Zhu and X. Pan, *Inorg. Chem. Commun.*, 2012, **22**, 137–140.
10 K. Wang, Y. He, Y. Zhao, P. Ma and J. Wang, *J. Mol. Struct.*, 2019, **1195**, 184–188.
11 Q. Lan, S.-J. Jin, Z. Wang, X.-Y. Li, Y. Xiong, Z.-C. Wang, S.-S. Liu, Z.-M. Zhang and Q. Zhao, *Tungsten*, 2024, **6**, 447–453.
12 N. I. Gumerova and A. Rompel, *Chem. Soc. Rev.*, 2020, **49**, 7568–7601.
13 A.-A. Mamdouh, A. B. M. Ibrahim, N. E.-H. A. Reyad, T. R. Elsayed, I. C. Santos, A. Paulo and R. M. Mahfouz, *J. Cluster Sci.*, 2023, **34**, 1535–1546.
14 J. D. Somasundaram, A. Ebrahimi, S. P. Nandan, A. Cherevan, D. Eder, M. Šupolíková, E. Nováková, R. Gyepes and L. Krivosudský, *J. Inorg. Biochem.*, 2023, **239**, 112067.
15 I. Msaadi, A. Rayes, M. Benito, N. Issaoui, E. Molins and B. Ayed, *J. Mol. Struct.*, 2022, **1262**, 133085.
16 H. Naslhajian, M. Amini, S. M. F. Farnia, A. Sheykhi, O. Ş ahin and O. Z. Yeşilel, *J. Coord. Chem.*, 2017, **70**, 2940–2949.
17 J. M. Missina, L. B. P. Leme, K. Postal, F. S. Santana, D. L. Hughes, E. L. de Sá, R. R. Ribeiro and G. G. Nunes, *Polyhedron*, 2020, **180**, 114414.
18 S. Li, P. Wang, K. Yang, Y. Liu, D. Cheng and L. He, *Dyes Pigm.*, 2023, **211**, 111083.
19 D. H. Kita, G. A. de Andrade, J. M. Missina, K. Postal, V. K. Boell, F. S. Santana, I. F. Zattoni, I. d S. Zanzarini, V. R. Moure, F. G. d M. Rego, G. Picheth, E. M. de Souza, D. A. Mitchell, S. V. Ambudkar, G. G. Nunes and G. Valdameri, *FEBS Lett.*, 2022, **596**, 381–399.
20 G. Sridharan and A. A. Shankar, *Int. J. Oral Maxillofac. Pathol.*, 2012, **16**, 251–255.
21 D. Wang, H. H. Kung and M. A. Barteau, *Appl. Catal., A*, 2000, **201**, 203–213.
22 C. F. Macrae, I. Sovago, S. J. Cottrell, P. T. A. Galek, P. McCabe, E. Pidcock, M. Platings, G. P. Shields, J. S. Stevens, M. Towler and P. A. Wood, *J. Appl. Crystallogr.*, 2020, **53**, 226–235.
23 Bruker, Bruker APEX3, Bruker AXS Inc., Madison, Wisconsin, USA, 2015.

24 G. Sheldrick, *Acta Crystallogr., Sect. A: found. Adv.*, 2015, **71**, 3–8.
25 P. J. Brown, A. G. Fox, E. N. Maslen, M. A. O'Keefe and B. T. M. Willis, Intensity of diffracted intensities, *International Tables for Crystallography*, 2006, vol. C, pp. 554–595.
26 X. Xu and W. A. Goddard, *Proc. Natl. Acad. Sci.*, 2004, **101**, 2673–2677.
27 F. Weigend and R. Ahlrichs, *Phys. Chem. Chem. Phys.*, 2005, **7**, 3297–3305.
28 F. Neese, *Wiley Interdiscip. Rev.: Comput. Mol. Sci.*, 2012, **2**, 73–78.
29 F. Neese, *Wiley Interdiscip. Rev.: Comput. Mol. Sci.*, 2018, **8**, e1327.
30 A. V. Marenich, C. J. Cramer and D. G. Truhlar, *J. Phys. Chem. B*, 2009, **113**, 6378–6396.
31 Y. Niu, Q. Peng, C. Deng, X. Gao and Z. Shuai, *J. Phys. Chem. A*, 2010, **114**, 7817–7831.
32 Q. Peng, Y. Niu, C. Deng and Z. Shuai, *Chem. Phys.*, 2010, **370**, 215–222.
33 B. de Souza, F. Neese and R. Izsák, *J. Chem. Phys.*, 2018, **148**, 034104.
34 T. Petrenko, S. Kossmann and F. Neese, *J. Chem. Phys.*, 2011, **134**, 054116.
35 N. Bošnjaković-Pavlović, J. Prévost and A. Spasojević-de Biré, *Cryst. Growth Des.*, 2011, **11**, 3778–3789.
36 A. García-García, L. Noriega, F. J. Meléndez-Bustamante, M. E. Castro, B. L. Sánchez-Gaytán, D. Choquesillo-Lazarte, E. González-Vergara and A. Rodríguez-Diéguez, *Inorganics*, 2021, **9**, 67.
37 R. Dridi, Z. Abdelkafi-Koubaa, N. Srairi-Abid, B. Socha and M. F. Zid, *J. Inorg. Biochem.*, 2024, **255**, 112533.
38 C. Yuan, L. Lu, M. Zhu, Q. Ma and Y. Wu, *Acta Crystallogr., Sect. E: Struct. Rep. Online*, 2009, **65**, m267–m268.
39 Y. Gong, C. Hu, H. Li, W. Tang, K. Huang and W. Hou, *J. Mol. Struct.*, 2006, **784**, 228–238.
40 L. Bartošová, Z. Padělková, E. Rakovský and P. Schwendt, *Polyhedron*, 2012, **31**, 565–569.
41 S. R. Amanchi and S. K. Das, *Front. Chem.*, 2018, **6**, 469.
42 A. S. Rao, T. Arumuganathan, V. Shivaiah and S. K. Das, *J. Chem. Sci.*, 2011, **123**, 229–239.
43 E. Sánchez-Lara, B. Martínez-Valencia, N. D. Corona-Motolinia, B. L. Sanchez-Gaytan, M. E. Castro, S. Bernès, M. A. Méndez-Rojas, F. J. Meléndez-Bustamante and E. González-Vergara, *New J. Chem.*, 2019, **43**, 17746–17755.
44 B. Wu, X. Xu, K. Chen, Z. Xiao and P. Wu, *Z. Kristallogr. - New Cryst. Struct.*, 2015, **230**, 353–355.
45 E. Sánchez-Lara, A. Pérez-Benítez, S. Treviño, A. Mendoza, F. J. Meléndez, E. Sánchez-Mora, S. Bernès and E. González-Vergara, *Crystals*, 2016, **6**, 65.
46 E. Sánchez-Lara, I. Sánchez-Lombardo, A. Pérez-Benítez, Á. Mendoza, M. Flores-Álamo and E. G. Vergara, *J. Cluster Sci.*, 2015, **26**, 901–912.
47 P. F. Avila, T. J. Ripplinger, D. J. Kemper, J. L. Domine and C. D. Jordan, *J. Phys. Chem. Lett.*, 2019, **10**, 6032–6037.
48 Y. Ikemoto, Y. Harada, M. Tanaka, S.-N. Nishimura, D. Murakami, N. Kurahashi, T. Moriwaki, K. Yamazoe, H. Washizu, Y. Ishii and H. Torii, *J. Phys. Chem. B*, 2022, **126**, 4143–4151.
49 N. Sundaraganesan, C. Meganathan and M. Kurt, *J. Mol. Struct.*, 2008, **891**, 284–291.
50 M. A. Nasher, M. I. Youssif, N. A. El-Ghamaz and H. M. Zeyada, *Optik*, 2019, **178**, 532–543.
51 O. V. Ovchinnikov, A. V. Evtukhova, T. S. Kondratenko, M. S. Smirnov, V. Y. Khokhlov and O. V. Erina, *Vib. Spectrosc.*, 2016, **86**, 181–189.
52 A. Kahn-Harari, R. E. Ballard and E. K. Norris, *Acta Crystallogr., Sect. B: Struct. Crystallogr. Cryst. Chem.*, 1973, **29**, 1124–1126.
53 G. Xue, J. Xiong, H. Guo, G. Cao, S. Nie and H. Hu, *Electrochim. Acta*, 2012, **69**, 315–319.
54 S. Nie, Y. Zhang, B. Liu, Z. Li, H. Hu, G. Xue, F. Fu and J. Wang, *J. Solid State Chem.*, 2010, **183**, 2957–2962.
55 L. O. Kostjukova, S. V. Leontieva and V. V. Kostjukov, *J. Mol. Liq.*, 2021, **336**, 116369.
56 S. Jockusch, N. J. Turro and D. A. Tomalia, *Macromolecules*, 1995, **28**, 7416–7418.
57 A. Fernández-Pérez and G. Marbán, *ACS Omega*, 2020, **5**, 29801–29815.
58 J. C. Dean, D. G. Oblinsky, S. R. Rather and G. D. Scholes, *J. Phys. Chem. B*, 2016, **120**, 440–454.
59 M. Rabbani, Z. S. Seghatoleslami and R. Rahimi, *J. Mol. Struct.*, 2017, **1146**, 113–118.
60 Y.-H. Fan, Y.-X. Li, W.-J. Zhu, Y. Bai and D.-B. Dang, *Dyes Pigm.*, 2023, **216**, 111363.
61 Y. Umemura, E. Shinohara and R. A. Schoonheydt, *Phys. Chem. Chem. Phys.*, 2009, **11**, 9804–9810.
62 A. Bain, P. Chandna, G. Butcher and J. Bryant, *J. Chem. Phys.*, 2000, **112**, 10435–10449.
63 M. Ilanchelian, C. Retna Raj and R. Ramaraj, *J. Inclusion Phenom. Macrocyclic Chem.*, 2000, **36**, 9–20.
64 M. Kahloul, S. Mahfoudhi, J. Chekir and A. Hafiane, *Environ. Dev. Sustainability*, 2020, **22**, 4655–4672.
65 N. Martin and Y. Leprince-Wang, *Phys. Status Solidi A*, 2021, **218**, 2100532.
66 L. O. Kostjukova, S. V. Leontieva and V. V. Kostjukov, *J. Mol. Graphics Modell.*, 2021, **107**, 107964.
67 Y. Shi, X. Wang, X. Wang, K. Carlson and Z. Li, *Crystals*, 2021, **11**, 1181.
68 J. M. Small and H. Hintelmann, *Anal. Bioanal. Chem.*, 2007, **387**, 2881–2886.